 MCB, vol.1, no.1, pp.69-80, 2004

System Optimization for the Development of Ultrasensitive Electronic Biosensors Using Carbon Nanotube Nanoelectrode Arrays

Jessica E. Koehne, Jun Li[1], Alan M. Cassell, Hua Chen, Qi Ye, Jie Han, and M. Meyyappan

Abstract: Vertically aligned multi-walled carbon nanotubes (MWCNTs) have been reported in fabricating nanoelectrode arrays. Further studies on optimizing this system for the development of ultrasensitive DNA sensors are reported here. The mechanical stability of the as-grown MWCNT array can be improved by polymer coating or SiO_2 encapsulation. The latter method provides excellent electronic and ionic insulation to the sidewall of MWCNTs and the underlying metal layer, which is investigated with electrochemical impedance spectroscopy. The insulation ensures well-defined nanoelectrode behavior. A method is developed for selectively functionalizing biomolecules at the open end of MWCNTs while keeping the SiO_2 surface passivated, using the unique graphitic chemistry. An ultrahigh sensitivity approaching the limit of fluorescence techniques is obtained with this system for DNA detection.

1 Introduction

Electrochemical (EC) methods are attractive techniques for molecular analysis of biological samples [Kuhr, 2000; Umek, 2001; Boon, 2000; Popovich, 2002], which can be directly integrated with microelectronics and microfluidics devices to gain advantages in miniaturization, multiplexing, and automation [Sosnowski, 1997]. Recently, many studies have reported the modification of the electrode surface with organic monolayers or nanostructured sensing elements to enhance biosensing ability. In a series of reports [Li, 2003a; Koehne, 2003; Koehne, 2004], we have demonstrated that vertically aligned multiwalled carbon nanotubes (MWCNTs) embedded in a SiO_2 matrix could be employed as well-defined nanoelectrode arrays (NEAs) for ultrasensitive DNA detection. Specific hybridization of PCR amplicons of the BRCA1 gene as well as oligonucleotide targets were measured by the combination of the MWCNT NEAs with $Ru(bpy)_3^{2+}$ mediated guanine oxidization [Li, 2003a; Koehne, 2003]. An ultrahigh sensitivity approaching the limit of fluorescence techniques was achieved [Koehne, 2003]. This makes it possible to realize the advantages of electronic biosensing technologies for applications requiring rapid results. Here we report further studies on optimizing the MWCNT NEA platform for the development of biosensors, with particular emphasis on the following issues: (1) the mechanical stability, (2) electrical characteristics, and (3) chemical selectivity and reliability for surface functionalization/passivation.

There are many reports on using carbon nanotube (CNT) arrays or random ensembles as electrodes for electrochemical sensors [Ng, 2001; Guiseppi-Elie, 2002; Gooding, 2003; Yu, 2003, Sotiropoulou, 2003]. However, such raw CNT arrays or ensembles have poor mechanical stability (particularly apt to bunch due to the capillary force of liquid droplets) [Li, 2002a; Chen, 2002] and high electronic noise due to the large surface area [Koehne, 2004; Li, 2002a; Chen, 2002]. The chemistry is also complicated due to the complex nanostructure. In contrast, a critical step was introduced in our fabrication of NEAs [Li, 2002b, 2003; Koehne, 2003, 2004], which encapsulates the as-grown MWCNT array in a SiO_2 matrix by chemical vapor deposition (CVD) of tetraethylorthosilicate (TEOS). This method improves the mechanical stability of the MWCNT array dramatically so that an aggressive chemical mechanical polishing (CMP) process can be applied to planarize the top surface and expose only a fraction of the MWCNTs [Koehne, 2003]. Together, these processing steps make it possible to fabricate reliable and well-defined MWCNT NEAs for biosensor development. In this report, we further address the properties of the NEAs from an electronic signaling and surface chemistry points of view. Electrochemical impedance spectroscopy (EIS) is employed to illustrate the equivalent circuit of MWCNT

[1] Center for Nanotechnology, NASA Ames Research Center, Moffett Field, CA 94035, USA Fax: 1-(650)604-5244; Tel: 1-(650)604-6459; E-mail: jli@mail.arc.nasa.gov

NEAs. Selective passivation and functionalization methods are demonstrated to reduce non-specific adsorption and improve the reliability for biosensing. These studies are important for optimizing the sensitivity and reliability, which allow us to reach a sensitivity for DNA detection approaching the limit of conventional fluorescence techniques.

2 Experimental Methods

Electrode preparation. Randomly distributed MWCNT NEAs are fabricated on silicon chips using a bottom-up scheme reported previously [Li, 2003; Koehne, 2003; Koehne, 2004], as illustrated in Figure 1. The typical sample size is $\sim$1x1 cm^2. The processing steps include: (1) deposition of the underlying metal layer ($\sim$200 nm Cr or Pt) and a catalyst film ($\sim$20-30 nm Ni) by ion beam sputtering, (2) MWCNT array growth by DC biased plasma enhanced chemical vapor deposition (PECVD) [Ren, 1998; Cruden, 2003], (3) SiO_2 encapsulation by TEOS CVD in a tube furnace at 715° C under $\sim$400 mTorr TEOS vapor, and (4) CMP with a vibratory polisher (Vibromet 2, Buehler, IL). As we demonstrated before [Koehne, 2003], the density of exposed MWCNT nanoelectrodes can be controlled by stopping CMP at the proper stage, which is critical for the performance of the sensors. The MWCNT NEA is then electrochemically etched at 1.5 V vs saturated calomel electrode (SCE) in 1.0 M NaOH to produce a well-defined surface [McCreery, 1991] before it is used for further treatment. The samples are examined with scanning electron microscopy (SEM) (S4000, Hitachi, Japan) after each step of this procedure.

Electrochemical characterization and DNA detection. Cyclic voltammetry (CV), AC voltammetry (ACV), and EIS are carried out with an Autolab potentiostat (GSTAT12, Ecochemie, The Netherlands) in a three-electrode setup using a Pt coil counter electrode (c.e.) and a SCE reference electrode (r.e.) (as shown in Fig. 1). The size of the working electrode (w.e.) is defined with a 3 mm i.d. O-ring sealed in a TEFLON cell. ACV is measured with an AC sinusoidal wave at 10 Hz and 25 mV amplitude superimposed on the staircase DC potential ramp. EIS is carried out at the open circuit potential (OCP) in 1.0 M KCl by applying 10 mV sinusoidal AC potential waves with the frequency varying from 10 kHz to 1 mHz uniformly in the logarithm scale. The EIS data is fit using the Autolab frequency

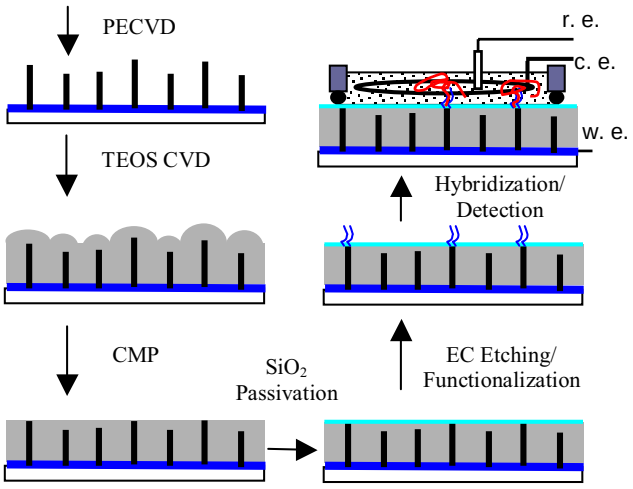

Figure 1 : The fabrication procedure for electronic DNA sensors based on MWCNT nanoelectrode arrays.

response analysis (FRA) package. EC DNA hybridization tests are performed by ACV in 5.0 mM $Ru(bpy)_3^{2+}$ with 0.20 M NaOAc buffer (pH=5.2) using a DC potential ramp from 0.50 to 1.20 V. A highly oriented pyrolytic graphite (HOPG) electrode is used as a model electrode for comparison. It is prepared by sealing a small piece of HOPG ($\sim$1x1x10 mm^3, Advanced Ceramics, Germany) with epoxy in a 3 mm i.d. glass tube. One end is polished to expose the $\sim$1x1 mm^2 edge-plane and another end is connected to a piece of copper wire with Gallium inside the glass tube.

Biosensing assay. The following procedures are employed in biosensing:

a. SiO_2 surface passivation. The MWCNT NEA is immersed in a 1% 3-aminopropyltriethyoxysilane (Aldrich, WI, USA) in ethanol solution for 20 minutes producing a primary amine surface functionality [Cui, 2001]. 50 μL of a 0.1 mM 2-(2-methoxyethoxy)acetic acid solution is mixed with 5 mg 1-ethyl-3(3-dimethyl aminopropyl)carbodiimide hydrochloride (Fluka, Switzerland) and 2.5 mg N-hydroxysulfo-succinimide (Aldrich, WI, USA) which act as coupling reagents [Staros, 1982]. The solution is applied to the functionalized MWCNT nanoelectrode array and incubated at room temperature for 1 hour. The primary amine from the functionalized surface forms an amide bond with the carboxylic acid group from the 2-(2-methoxyethoxy)acetic acid, resulting in a surface terminated with ethylene glycol moieties. The

sample is then thoroughly rinsed with water.

b. Probe functionalization. The passivated MWCNT nanoelectrode array is then electrochemically etched at 1.5 V (vs. SCE) for about 120 s in 1 M NaOH, which selectively removes the molecules attached during the passivation steps as well as some carbon atoms at the exposed end of MWCNTs, thus reactivating the electrodes. The etched MWCNTs are dominated with carboxylic acid and hydroxyl groups [McCreey, 1991]. A 10 μM oligonucleotide probe, [Cy3]5'-CTIIATTTCICAIITCCT-3" [AmC7-Q] (QIAGEN, CA, USA), in 50 μL phosphate buffered saline (PBS) (Sigma, St. Loius, USA), is mixed with the coupling reagents (0.5 mg 1-ethyl-3(3-dimethylaminopropyl)carbodiimide hydrochloride (Fluka, Switzerland) and 0.25 mg N-hydroxysulfo-succinimide (Aldrich, WI, USA)). Electroactive guanine bases are substituted by nonelectroactive inosine bases in the probe DNA. The reaction mixture is applied to the MWCNT NEA and incubated at room temperature for about 1 hour [Nguyen, 2002]. The sample is then thoroughly rinsed with PBS.

c. Target hybridization. The target oligonucleotide, with a sequence:

[Cy5]
5'-AGGACCTGCGAAATCCAG**GGGGGGGGGG**-3' (QIAGEN, CA, USA),

consisting of an additional 10 guanine bases as EC signal moieties is hybridized by incubating the probe-functionalized electrodes in $\sim$0.1 μM target solutions in 3x saline sodium citrate (SSC) buffer over 2 hours at 40°C.

d. Stringent washing. In the case of samples without SiO_2 surface passivation, the adsorbed biomolecules present from nonspecific binding need to be removed by stringent washes using a three-step procedure. Three different SSC buffers (Sigma, St. Loius, USA), which include: (1) 2x SSC with 0.1% sodium dodecyl sulfate (SDS), (2) 1x SSC, and (3) 0.1x SSC, respectively. The sample is shaken in each buffer at 40° C for 15 minutes, with a thorough rinse in between each stringent washing step. Fluorescence images of both Cy3 and Cy5 are taken with a laser scanner (GMS 417, Genetic Micro Systems, MA, USA) to monitor the binding of biomolecules on the electrode surface.

3 Results and Discussions

Figure 2(a) shows the SEM image of an as-grown MWCNT array on the chip surface. Each MWCNT is well aligned along the surface normal with the aid of the electrical field present during PECVD [Ren, 1998; Cruden, 2003, Cassell, 2004, Merkulov, 2002]. The MWCNTs form a randomly distributed array with a rather narrow distribution in diameter (with the standard deviation $\sim$17% of the mean value), the mean value of which can be approximately varied from 30 to 100 nm. The diameter is essentially the same along the tube axis. The length can be controlled from $\sim$1 to 15 μm by varying the reaction time. High-resolution transmission electron microscopy shows that they are bamboo-like defective MWCNTs with the graphitic layers not ideally parallel to the tube axis [Ren, 1998], sometimes referred to as "carbon nanofibers" [Merkulov, 2002]. As we reported before [Koehne, 2004], such MWCNT array has a huge active surface area which produces a double-layer capacitance of $\sim$30 mF/cm^2, about 500 times that of a HOPG edge-plane electrode ($\sim$60 μF/cm^2) [McCreey, 1991]. Even though such 3D porous nanostructures can be directly used to immobilize biomolecules in some biosensor studies [Guiseppi-Elie, 2002; Gooding, 2003; Yu, 2003; Sotiropoulou, 2003], reliability is a concern due to the low mechanical strength, and large non-specific chemical adsorptions. As shown in Fig. 2(b), raw MWCNTs collapse into microbundles after dipping into liquids. The collapse is mostly attributed to the lateral cohesive capillary force by the solvent during the drying process, rather than the hydrophobic-hydrophilic interactions, since various solvents with quite different polarities including water, ethanol, acetone, and hexane produce similar results.

The mechanical strength of the MWCNT array can be improved by coating with a thin polymer film. Figure 2(c) shows the SEM image of a MWCNT array (from the same batch used in Fig. 2(a)) after electropolymerization in 0.05 M pyrrole solution with 1.0 M KCl supporting electrolyte at 1.0 V for 150 s. It produces a uniform polypyrrole (Ppy) coating with $\sim$40 to 50 nm thickness similar to a previous report [Chen, 2001, 2002]. Surprisingly, the MWCNT array maintains its original alignment after drying in air. Clearly, the thin polymer coating is enough to form a robust sheath and dramatically improve the mechanical strength of the individual MWCNTs. Our Raman study shows that the Ppy film

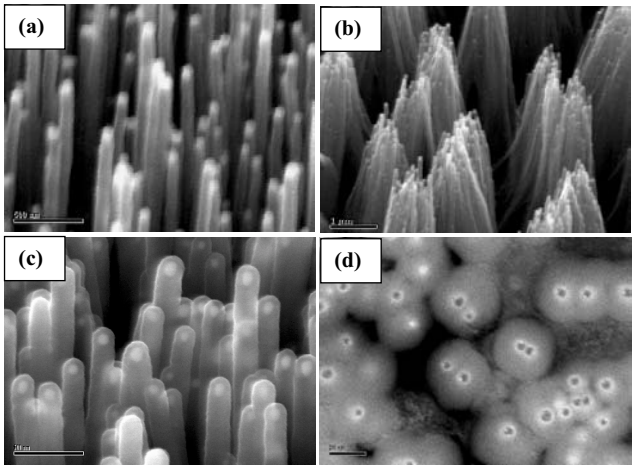

Figure 2 : SEM images of (a) an as-grown vertically aligned MWCNT array, (b) the MWCNT array after dipping into liquids, (c) the MWCNT array after coating with a uniform polypyrrole film by electropolymerization, and (d) the exposed ends of MWCNT array embedded in SiO_2 after planarization with chemical mechanical polishing. (a)-(c) are perspective views at 45° angle and (d) is the top view. The scale bars are 500 nm, 1 μm, 500 nm, and 200 nm, respectively.

on the MWCNT array presents extraordinarily high bipolaron population relative to conventional Ppy films, indicating the extremely high electrical conductivity [Chen, unpublished]. This is likely due to longer and more ordered conjugated Ppy chains electropolymerized on the well-defined MWCNT nanotemplates, which also provides much higher mechanical strength.

Fig. 2(c) also indicates that the MWCNT array maintains its original alignment as long as it is not taken out from aqueous solutions. The collapsing only happens during the drying process. The in-situ deposition of a conductive polymer film can protect the integrity of the intriguing 3D nanostructure for repeated use in biological media. In addition, the polymer coating can be effectively used to modify the MWCNT surface from hydrophobic to hydrophilic, which is desired for avoiding non-specific binding, while facilitating surface functionalization using specific biomolecular probes [Shim, 2002]. Such systems can be directly used for immunosensors or enzymatic sensors where immobilization of more biomolecules is desired [Gao, 2003]. The conductive polymer coating, however, has one drawback due to the high permeability of polymer films, causing a large background noise. A Ppy coated MWCNT array typically shows a capacitance value several times bigger than the original MWCNT sample [Chen, 2001, 2002].

In an effort to develop ultrasensitive DNA sensors, the number of DNA molecules to be detected is minimal, resulting in very low signals. As a result, minimizing the background noise is critical in system design for maximizing the sensitivity, i.e. the signal-to-noise ratio. A nanoelectrode [Penner, 1990; Fan, 1995] based on the ultramicroelectrode (UME) concept [Wightman, 1981], i.e. with the critical dimension less than the scale of the diffusion layer (typically over six times of the electrode radius), would be an attractive platform for this application. The temporal and spatial resolution can be improved by orders of magnitude by decreasing the size of the electrodes from microns to nanometers [Penner, 1990; Fan, 1995]. NEAs are of particular interest due to the ease in use and high reliability. This approach requires a good insulation of both electronic and ionic conductance at the sidewall and underlying metal lines. With our innovation, NEAs can be reliably fabricated by combining the recent developments in carbon nanotube nanotechnologies with well established TEOS CVD processing. The SEM image of such an electrode is shown in Fig. 2(d). Clearly, SiO_2 encapsulates all MWCNTs and the underlying metal surface. CMP planarizes this insulating matrix and exposes the very end of a portion of MWCNTs. The density of active MWCNT NEAs can be controlled by stopping CMP at the proper stage [Koehne, 2003]. A plasma etching process has also been reported to expose CNTs [Guillorn, 2001]. In previous reports [Li, 2003a; Koehne, 2004], we have demonstrated that each exposed MWCNT behaves nearly as an independent nanoelectrode for measuring redox species in the solution if the total density is less than $\sim 1 \times 10^8$ electrodes/cm^2. At higher densities, the diffusion layers of neighboring nanoelectrodes start to overlap, resulting in a CV curve similar to a solid macroelectrode.

EIS is a useful technique to illustrate the physical properties of the electrode surface in terms of equivalent circuits [Macdonald, 1987]. Particularly, the data obtained in the absence of redox species directly reflects both the electronic and ionic insulating properties of SiO_2 prepared by TEOS CVD, which was reported to present microdefects [Kato, 1994]. EIS measurements with AC waves from 10 kHz to 1 mHz are carried out in 1.0 M KCl to derive

Table 1 : Fitting Parameters for the EIS data of Three Electrodes using equivalent circuit in Fig. 3(b).

Electrode	R_s (Ω cm^2)	R_f (MΩ cm^2)	CPE		Calculated Carbon Area (mm^2)
			Y_0 (x10^{-5})	α	
HOPG Edge	0.579 ±0.012	0.381 ±0.031	17.19 ±0.27	0.879 ±0.002	0.99
h-dNEA[a]	18.79 ±0.16	1.038 ±0.077	1.014 ±0.018	0.822 ±0.001	0.018[c]
l-dNEA[b]	31.70 ±0.65	2.184 ±0.082	0.0951 ±0.0023	0.820 ±0.002	0.0069[c]

a. The low-frequency data between 3.36 mHz and 1 mHz are not included for fitting.
b. The low-frequency data between 2.77 mHz and 1 mHz are not included for fitting.
c. By assuming the average size of MWCNTs is 50 nm in diameter.

the basic equivalent circuit. Fig. 3 shows the EIS data obtained with a $\sim$1 mm^2 HOPG edge-plane electrode (HOPG edge), a high-density MWCNT nanoelectrode array (h-dNEA) (with $\sim$1.3x10^8 electrodes/cm^2) and a low-density MWCNT nanoelectrode array (l-dNEA) (with $\sim$2-5x10^7 electrodes/cm^2). The data normalized to the geometric surface area is presented as Bode plots and Nyquist plot in Fig. 3, where Z represents the total impedance with Z' and Z" corresponding to its real and imaginary part, respectively [Bard, 2001].

Clearly, the data set shifts systematically to higher frequency in Fig. 3(a) following the trend of HOPG edge (+), h-dNEA (open circles), and l-dNEA (filled circles). All data can be nicely fit with a simple Randles circuit [Bard, 2001] shown in the inset of Fig. 3(b) with a constant phase element (CPE) [Macdonald, 1987] in parallel with a faradaic reaction resistance (R_f) in addition to the ohmic resistance of the solution (R_s). The impedance of a CPE is given by

$$Z = 1/(Y_0 i\omega)^{\alpha} \quad (1)$$

Where ω is the angular frequency (ω=2πf) and f is the conventional frequency in Hz. The exponent α is typically between 0.8 to 1.0 for solid electrodes and the CPE behaves as a capacitor when α=1.0. Table 1 lists all the fitting parameters using the equivalent circuit shown in the inset of Fig. 3(b).

A CPE is necessary since EIS data of all three electrodes in Nyquist plots (as shown in Fig. 3(c)) are depressed in the vertical axis from an ideal semicircle, which cannot be fit with ideal capacitors. The parallel resistance R_f indicates the existence of a small faradaic reaction likely due to the electroactive oxygen-containing groups at the broken edge of the graphitic sheets. The phase angle in the medium frequency range presents a plateau with constant values as shown in Fig. 3(b). The values are about 80°, 74°, and 73°, for HOPG edge, h-dNEA, and l-dNEA, respectively. While the constant phase of MWCNT NEAs is clearly lower than that of HOPG edge, the curve also shifts to higher frequencies as the nanoelectrode density decreases. The α values of NEAs are about the same at 0.82, but clearly lower than 0.88 from HOPG edge. The Nyquist plot in Fig. 3(c) shows a clear trend that the impedance increases with a decrease in nanoelectrode density.

The fitting parameters clearly indicate that there is a distinction between macroscopic HOPG edge-plane electrodes and MWCNT NEAs. Table 1 lists the calculated total area of exposed MWCNTs in comparison to HOPG edge. The difference in R_s, R_f, and α between HOPG and MWCNT NEAs is not just a scaling factor as those between two NEAs. The EIS data of NEAs at low frequencies ($\leq\sim$3 mHz, about 5 data points) always gave larger values than the calculated number and therefore are not included in data fitting. The data obtained from the HOPG edge, however, can be nicely fit in the whole frequency range from 10 kHz to 1 mHz. Considering that NEAs are more sensitive to molecule adsorptions, it is not surprising that the low-frequency data which takes much longer time to measure may not be reliable.

The deviation from Helmholtz parallel plate capacitor to CPE has been attributed to the surface roughness or inhomogeneous reactivity in the literature [Mulder, 1990; Kim, 2003], both of which may be valid for MWCNT NEAs. First, the surface of the SiO_2 matrix in NEAs as shown in Fig. 2(d) has a roughness of $\sim$10 nm, which is larger than normal solid electrodes. Careful CMP to planarize the electrode surface is indeed important. The

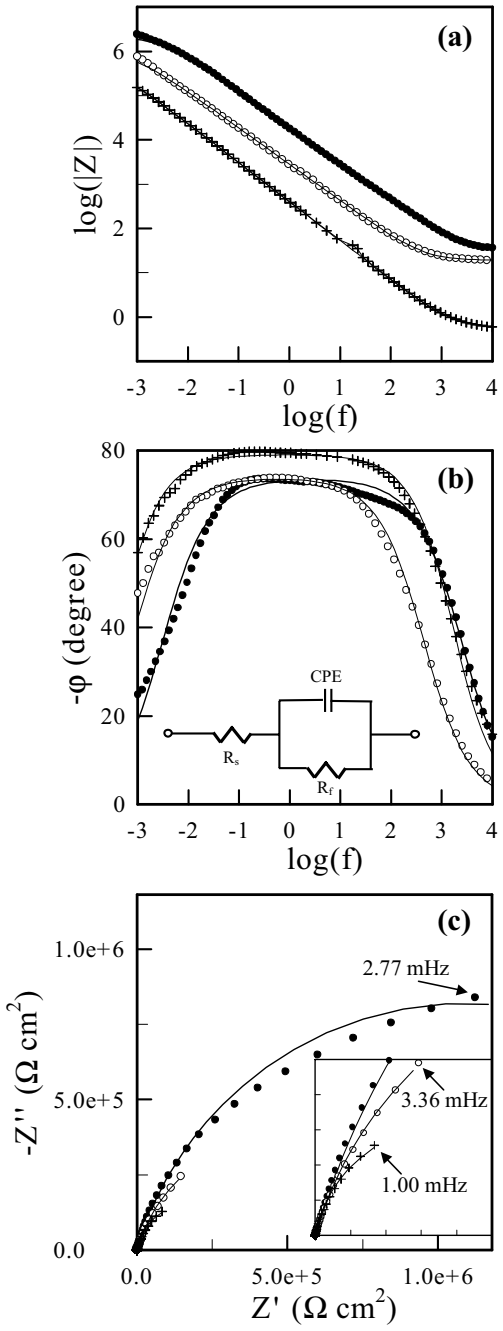

Figure 3 : The electrochemical impedance spectroscopy of a ~1 mm^2 HOPG edge plane electrode (shown in +), a high-density MWCNT nanoelectrode array embedded in SiO_2 (with ~1.3x10^8 electrodes/cm^2, shown in open circles), and a low-density MWCNT nanoelectrode array embedded in SiO_2 (with ~2-5x10^7 electrodes/cm^2, shown in black dots). All measurements were done at the open circuit potential in 1.0 M KCl with 10 mV sinusoidal waves with frequencies varying from 10 kHz to 1 mHz. (a) is Bode plot of the negative phase vs. the logarithm of the frequency f (in Hz), (b) is Bode plot of the logarithm of the absolute impedance (|Z| in Ω-cm^2) vs. the logarithm of the frequency f (in Hz), and (c) Nyquist plot of the real (Z') and imaginary (Z") parts of the impedance, respectively. Solid lines represent the fitting curves to the experimental data using the simple Randles equivalent circuit shown in the inset in (b). The inset in (c) shows the enlarged plots in the impedance amplitudes ranging from 0 to 2.5x10^5 (Ω cm^2).

3D roughness in other electrodes shown in Fig. 2(a)-(c) would complicate data analysis even further. Second, the inhomogeneity of surface chemistry is also a concern. Conventional carbon electrodes are irreproducible due to the fact that the amount of edge and basal orientations is not under control [McCreery, 1991]. Even the HOPG edge-plane electrode used in this study can form various oxygen-containing groups, which give varied electron transfer rates at different atomic sites. An EC etching procedure was found to be effective in producing –OH and –COOH dominated MWCNT ends similar to graphite edge-planes [McCreery, 1991]. Hence, even though the reaction sites are still inhomogeneous, MWCNT NEAs are among the most well-defined carbon electrodes whose EIS can be fit nicely with a simple equivalent circuit. The Y_0 value of the CPE decreases dramatically (by about 4 orders of magnitude) from HOPG edge to l-dNEA, indicating that the impedance at high frequencies may be used as a very sensitive and fast method for sensor development. Impedance techniques indeed have advantages in applications as high-speed biosensors [Yan, 2001] and neural probes [Rutten, 2001].

MWCNT NEAs may be compared to self-assembled monolayers (SAMs) on Au surfaces which are commonly used in many biosensor studies [Kuhr, 2000; Umek, 2001; Boon, 2000; Popovich, 2002]. Compact inert organic monolayers serve as the insulating matrix similar to SiO_2 in MWCNT NEAs. Even though the surface roughness is small, the EIS of a defect-free SAM on a polycrystalline Au electrode in the absence of redox species still needs to be fit with a CPE in series with a resistor [Boubour, 2000]. When defects or conducting molecules are introduced, more complex equivalent circuits involving at least two parallel RC circuits have to be used for data fitting [Boubour, 2000; Janek, 1998; Finklea, 1993]. A faradaic resistance on the order of a few $M\Omega cm^2$ was derived from the defective SAMs [Boubour, 2000], which is comparable to R_f in MWCNT NEAs. Clearly, both the electronic and ionic insulating properties of SiO_2 deposited by TEOS CVD are comparable to well-known compact SAMs.

The understanding of the MWCNT NEA in terms of a simple equivalent circuit is very helpful to fully utilize modern electronics techniques in electrochemical measurements for improving detection sensitivity. Since the signal is typically a faradaic current, with a very different phase compared to the background current which is mostly capacitive charging/discharging current, phase-sensitive techniques such as AC voltammetry (ACV) may discriminate them easily [Bard, 2001]. ACV is also attractive for obtaining an amplified signal from very small number of redox molecules [Umek, 2001].

Fig. 4 shows ACV measurements of h-dNEA containing 1.0 mM $K_4[Fe(CN)_6]$ in 1.0 M KCl with a 10 Hz AC wave at phase angles of 0°, 30°, 60°, and 90°, respectively. The peak at 0.22 V corresponds to the anodic oxidation of $K_4[Fe(CN)_6]$. Clearly, the results are phase-sensitive. The largest peak current and smallest background current are observed at 0°. As the phase shifts from 0° to 90°, the peak current decreases while the background current increases. This is consistent with the fact that the peak current is mainly in-phase faradaic current while the background is capacitive current with the phase close to 90°. The phase of a 10 Hz capacitive current would be at -74° in the absence of redox species as shown in Fig. 3(b). It may change if faradaic currents are involved. However, high sensitivity can normally be obtained at phase angles between 0° and 30°.

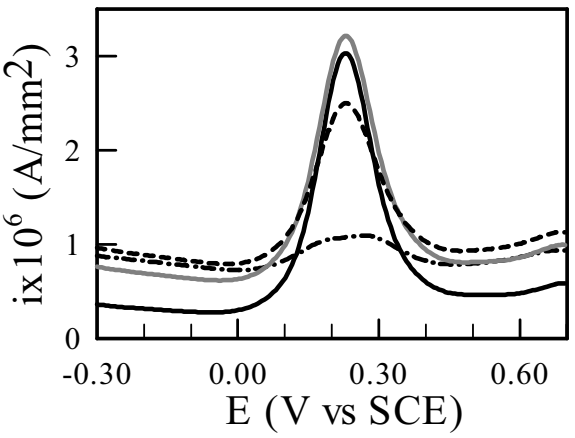

Figure 4 : AC voltammetry of a MWCNT nanoelectrode array (with ~2x10^9 electrodes/cm^2) in 1.0 M KCl with 1.0 mM $K_4[Fe(CN)_6]$ with the phase at 0° (black line), 30° (grey line), 60° (dashed line), and 90° (dash-dot line), respectively. A sinusoidal wave with 25 mV and 10 Hz is superimposed on a 20 mV/s staircase DC ramp from –0.30 V to 0.70 V.

Now that we have a well-defined MWCNT NEA, the next step is to immobilize biomolecular probes at de-

sired sites while keeping the rest of the surface passivated to avoid non-specific adsorption. A method is developed as shown in Fig. 5 to achieve such selective functionalization and passivation to MWCNT NEAs. As mentioned before, an as-prepared MWCNT NEA can be electrochemically etched to produce hydroxyl and carboxylic acid dominated MWCNT ends. The SiO_2 surface is terminated with hydroxyl groups as shown in Fig. 5. Aminopropyltriethyoxysilane is used to react with the hydroxyl groups and produces a monolayer with primary amine surface functionalities covering the whole surface (as depicted in Fig. 5(b)) [Cui, 2001]. 2-(2-methoxyethoxy)acetic acid is then applied to form an amide bond with the $–NH_2$ group facilitated by coupling reagents 1-ethyl-3(3-dimethyl aminopropyl) carbodiimide hydrochloride and N-hydroxysulfo-succinimide [Staros, 1982]. This generates a surface terminated with ethylene glycol (EG) moieties as shown in Fig. 5(c), which is known to resist non-specific adsorption of biomolecules [Ostuni, 2001]. The passivating molecules at the MWCNT ends can be removed by EC etching in 1.0 M NaOH, which regenerates a well-defined nanoelectrode surface dominated by –OH and –COOH groups. Primary amine terminated DNA probes or other biomolecules can then be attached to these specific sites through amide bonds as illustrated in Fig. 5(d).

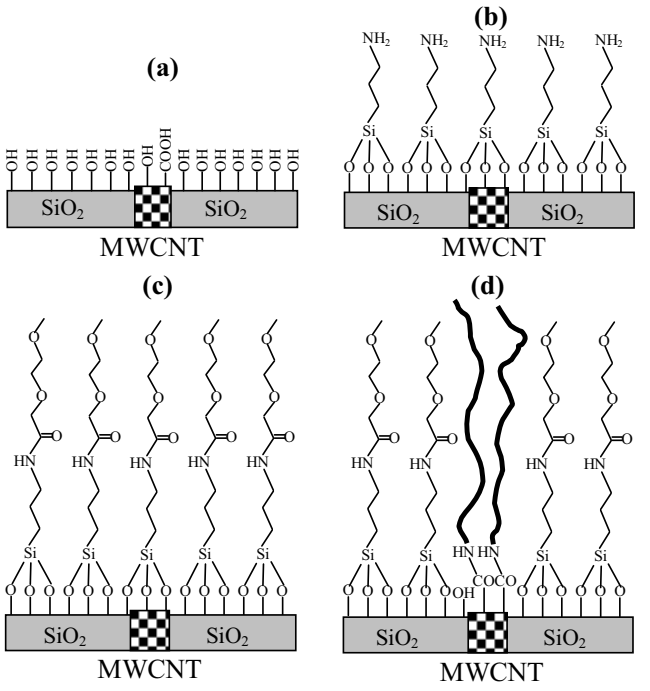

Figure 5 : The scheme for the surface passivation and selective functionalization of biomolecules to the embedded MWCNT nanoelectrode array. (a) A nonpassivated sample with the end of MWCNTs dominated by –OH and –COOH groups after electrochemical etch in 1.0 M NaOH. (b) An amine-terminated self-assembled monolayer formed through silanization with –OH groups on the surface. (c) An ethylene glycol surface generated through amide bonds for reducing non-specific adsorption. (d) Selective functionalization of biomolecular probes through amide bonds at electrochemically regenerated MWCNT ends. All schematics are not drawn to scale.

The effect of the surface passivation is shown by the fluorescence images in Fig. 6. Fig. 6(a) and 6(b) are taken from a nonpassivated MWCNT NEA after DNA probe functionalization and target hybridization, respectively. Strong fluorescence signals are observed over the entire surface due to significant non-specific adsorption, which cannot be removed by repeatedly rinsing with PBS or 3x SSC buffers. A three-step stringent wash using SDS has to be applied to get rid of the non-specific adsorption [Li, 2003a]. Similar fluorescence images were taken with the passivated MWCNT NEA following the scheme in Fig. 5. Clearly, a simple rinse step already removes non-specific adsorption more effectively than the extensive stringent washing with the non-passivated sample. Further stringent washing gives a very low Cy3 fluorescence signal from the probe molecules in Fig. 6(c), consistent with the fact that the MWCNT surface area is less than 1% in this NEA sample. The number of DNA targets hybridized on to the sample surface is even lower, whose Cy5 fluorescence signal is barely observed over the background noise in Fig. 6(d) and (e).

DNA sensors based on MWCNT NEAs can reach the limit of the sensitivity of fluorescence techniques [Li, 2003a, Koehne, 2003], which is demonstrated with the sample shown in Fig. 6(d) and (e). The results of electrochemical measurements with this sample immediately following the stringent washing are shown in Fig. 7. As we reported before, ACV measurements in 5.0 mM $Ru(bpy)_3^{2+}$ can give amplified signals for guanine oxidation. The oxidation signal of guanine bases brought to the electrode surface through specific hybridization superimposes on that of $Ru(bpy)_3^{2+}$, giving a well-defined

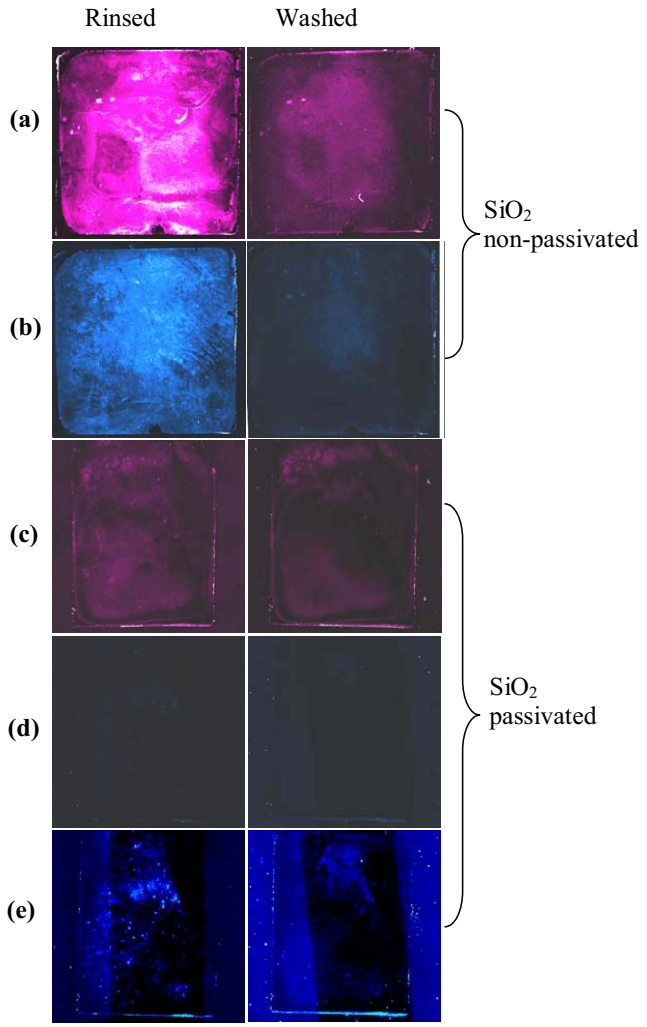

Figure 6 : The fluorescence image of MWCNT nanoelectrode arrays embedded in SiO_2 with the size of $\sim |x|$ cm^2 after the functionalization with a Cy3 tagged 18-mer oligonucleotide probe (a and c) and after the hybridization with a Cy5 tagged target (b, d, and e), by simply rinsing with 3x SSC buffer and three-step stringent washing, respectively. The SiO_2 surface in (a) and (b) is not passivated while that in (c)-(e) is coated with a self-assembled monolayer terminated with ethylene glycol moieties as shown in Fig. 5. The colors are arbitrarily assigned to the original grayscale data using pink to represent Cy3 and blue for Cy5. (a)-(d) are in the same output level, brightness, and contrast. The fluorescence signals in (d) are barely above the background noise, as illustrated in more detial in the extensively enhanced images in (e). Dark strips across the center of the images in (e) are due to the systematic instrumental noise of the laser scanner at the detection limit.

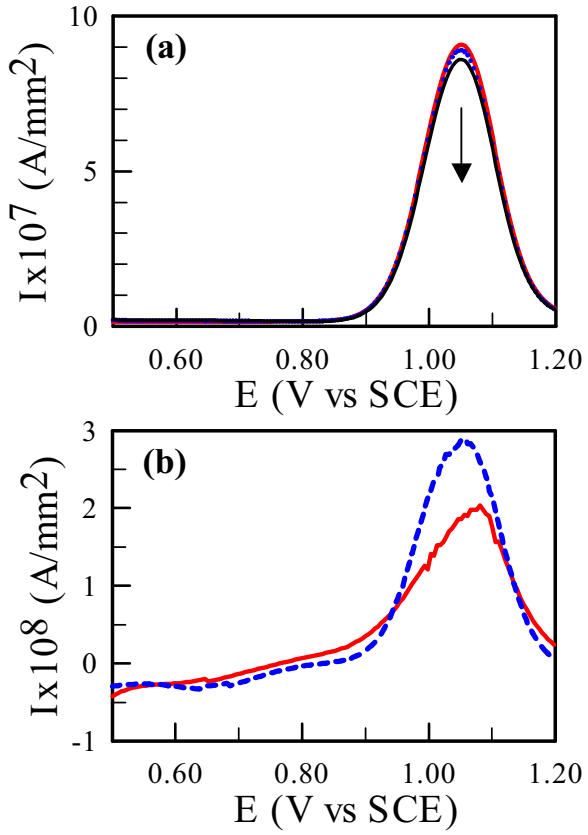

Figure 7 : (a) Three consecutive ACV measurements of a low-density MWCNT array after hybridization with 10-mer polyG tagged oligonucleotide targets in 5.0 mM $Ru(bpy)_3^{2+}$ and 0.20 M NaOAc (pH=5.2) using an AC sinusoidal wave at 10 Hz and 25 mV amplitude superimposed on the staircase DC potential ramp from 0.50 to 1.20 V at 20 mV/s. 1^{st} scan – thick red line, 2^{nd} scan – blue dot line, and 3^{rd} scan – thin black line. (b) The differential curve between 1^{st} and 2^{nd} scans (thick red line), 2^{nd} and 3^{rd} scans (blue dashed line), respectively.

peak current at 1.05 V. However, the guanine oxidation is irreversible and sine active guanine bases are consumed during each scan. As a result, the signal level keeps decreasing in subsequent scans as shown in Fig. 7(a). The differential signal between two consecutive scans is approximately proportional to the number of guanine bases being oxidized during former scan. A positive peak indicates that there are target DNAs brought to the surface by specific hybridization. Clearly, this signal is measurable even though the fluorescence signal is barely above the background in Fig. 6(d). In our previous studies us-

ing non-passivated NEAs, guanine bases are almost completely irreversibly oxidized in the first one or two scans, resulting in that the differential signal between the 2^{nd} and 3^{rd} scans is close to zero. This differential signal in Fig. 7(b), however, is even stronger than that between the first two scans. It is possible that guanine bases may go through more cycles in the SiO_2-passivated MWCNT NEAs, which is under further investigation now.

4 Conclusion

In summary, we have reported detailed studies on optimizing the MWCNT NEA for the development of ultrasensitive DNA sensors. The advantages in mechanical stability, electronics simplicity, and chemical selectivity for functionalization and passivation have been demonstrated. Ultrahigh sensitivity comparable to fluorescence techniques can be obtained with this system for DNA detection. Application of MWCNT NEAs for detecting other types of biomolecules can be explored based on these findings.

Acknowledgement: We acknowledge Dr. W. Fan for help on surface passivation and functionalization and Dr. Hou Tee Ng for participation in some of the fabrication work.

References

Bard, A. J.; Faulkner, L. R. (2001): *Electrochemical Methods: Fundamentals and Applications*, 2^{nd} Ed.; Wiley: New York, pp. 216-218.

Boon, E. M.; Ceres, D. M.; Drummond, T. G.; Hill, M. G.; Barton, J. K. (2000): Mutation detection by electrocatalysis at DNA-modified electrodes. *Nat. Biotechnol.*, vol. 18, pp. 1096-1100.

Boubour, E.; Lennox, R. B. (2000): Insulating properties of self-assembled monolayers monitored by impedance spectroscopy. *Langmuir*, vol. 16, pp. 4222-4228.

Boubour, E.; Lennox, R. B. (2000): Potential-induced defects in n-alkanethiol self-assembled monolayers monitored by impedance spectroscopy. *J. Phys. Chem. B*, vol. 104, pp. 9004-9010.

Cassell, A. M.; Ye, Q.; Cruden, B. A.; Li, J.; Sarrazin, P. C.; Ng, H. T.; Han, J.; Meyyappan, M. (2004): Combinatorial chips for optimizing the growth and integration of carbon nanofibre based devices. *Nanotechnology*, vol. 15, pp. 9-15.

Chen, B.; Li, J.; Delzeit, L.; Han, J.; Meyyappan, M. to be published.

Chen, J. H.; Huang, Z. P.; Wang, D. Z.; Yang, S. X.; Wen, J. G.; Ren, Z. F. (2001): Electrochemical synthesis of polypyrrole / carbon nanotube nanoscale composites using well-aligned carbon nanotube arrays. *Appl. Phys. A* vol. 73, pp. 129-131.

Chen, J. H.; Huang, Z. P.; Wang, D. Z.; Yang, S. X.; Li, W. Z.; Wen, J. G.; Ren, Z. F. (2002): Electrochemical synthesis of polypyrrole films over each of well-aligned carbon nanotubes. *Synthetic Metals*, vol. 125, pp. 289-294.

Cruden, B. A.; Cassell, A. M.; Ye Q.; Meyyappan, M. (2003): Reactor design considerations in the hot filament/direct current plasma synthesis of carbon nanofibers. *J. Appl. Phys.*, vol. 94(6), 4070-4078.

Cui, Y.; Wei, Q.; Park, H.; Lieber, C. M. (2001): Nanowire nanosensors for highly sensitive and selective detection of biological and chemical species. *Science*, vol. 293, pp. 1289-1292.

Fan, F.-R. F.; Bard, A. J. (1995): Electrochemical detection of single molecules. *Science*, vol. 267, pp. 871-874.

Finklea, H. O.; Snider D. A.; Fedyk, J.; Sabatani, E.; Gafni, Y.; Rubinstein, I. (1993): Characterization of octadecanethiol-coated gold electrodes as microarray electrodes by cyclic voltammetry and ac impedance spectroscopy. *Langmuir*, vol. 9, pp. 3660-3667.

Gao, M.; Dai, L.; Wallace, G. (2003): Biosensors based on aligned carbon nanotubes coated with inherently conducting polymers. *Electroanal.* vol. 11, pp. 1089-1094.

Gooding, J.J.; Wibowo, R.; Liu, J.; Yang, W.; Losic, D.; Orbons, S.; Mearns, F. J.; Shapter, J. G.; Hibbert, D. B. (2003): Protein electrochemistry using aligned carbon nanotube arrays. *J. Am. Chem. Soc.*, vol. 125, pp. 9006-9007.

Guillorn, M. A.; Melechko, A.; Merkulov, V. I.; Ellis, E. D.; Simpson, M. L.; Lowndes, D. H.; Baylor, L. R.; Bordonaro, G. J. (2001): Microfabricated field emission devices using carbon nanofibers as cathode elements. *J. Vac. Sci. Technol. B* vol. 19(6), pp. 2598-2601.

Guiseppi-Elie, A.; Lei, C.; Baughman, R. H. (2002): Direct electron transfer of glucose oxidase on carbon

nanotubes. *Nanotechnology* vol. 13, pp. 559-564.

Janek, R. P.; Fawcett, W. R.; Ulman, A. (1998): Impedance spectroscopy of self-assembled monolayers on Au(111): sodium ferrocyanide charge transfer at modified electrodes. *Langmuir*, vol. 14, pp. 3011-3018.

Kato, H.; Sakai, H.; Sugawara, K. (1994): Microdefects in oxide-films deposited on featured surfaces of VLSI substrates by thermal CVD of TEOS and O_2. *J. Electrochem. Soc.* vol. 141(11), pp. 3154-3157.

Kim, C. H.; Pyun, S. I.; Kim, J. H. (2003): An investigation of the capacitance dispersion on the fractal carbon electrode with edge and basal orientations. *Electrochimica Acta*, vol. 48, pp. 3455-3463.

Koehne, J.; Chen, H.; Li, J.; Cassell, A. M.; Ye, Q.; Ng, H. T.; Han, J.; Meyyappan, M. (2003): Ultrasensitive label-free DNA analysis using an electronic chip based on carbon nanotube nanoelectrode arrays. *Nanotechnology*, vol. 14, pp. 1239-1245.

Koehne, J.; Li, J.; Cassell, A.; Chen, H.; Ye, Q.; Ng, H. T.; Han, J.; Meyyappan, M. (2004): The fabrication and electrochemical characterization of carbon nanotube nanoelectrode arrays. *J. Mat. Chem.*, vol. 14(4), pp. 676-684.

Kuhr, W. G. (2000): Electrochemical DNA analysis comes of age. *Nat. Biotechnol.*, vol. 18, pp. 1042-1043.

Li, J.; Cassell, A. M.; Delzeit, L.; Han, J.; Meyyappan, M. (2002a): Novel three-dimensional electrodes: the electrochemical properties of carbon nanotube ensembles. *J. Phys. Chem. B*, vol. 106, pp. 9299-9305.

Li, J.; Stevens, R.; Delzeit, L.; Ng, H. T.; Cassell, A.; Han, J.; Meyyappan, M. (2002b): Electronic properties of multiwalled carbon nanotubes in an embedded vertical array. *Appl. Phys. Lett.*, vol. 81 (5), pp. 910-912.

Li, J.; Ng, H. T.; Cassell, A.; Fan, W.; Chen, H.; Ye, Q.; Koehne, J.; Han, J.; Meyyappan, M. (2003a): Carbon nanotube nanoelectrode array for ultrasensitive DNA detection. *Nano Letters*, vol. 3(5), pp. 597-602.

Li, J.; Ye, Q.; Cassell, A.; Ng, H. T.; Stevens, R.; Han, J.; Meyyappan, M. (2003b): A bottom-up approach for carbon nanotube interconnects. *Appl. Phys. Lett.*, vol. 82(15), pp. 2491-2493.

Macdonald, J. R. (1987): *Impedance Spectroscopy*, Wiley: New York.

McCreery, R. L. (1991): Carbon electrodes: structural effects on electron transfer kinetics. In: A. J. Bard (ed) *Electroanalytical Chemistry*; Marcel Dekker: New York; vol. 17, pp. 221-374.

Merkulov, V. I.; Melechko, A. V.; Guillorn, M. A.; Lowndes, D. H.; Simpson, M. L. (2002): Effects of spatial separation on the growth of vertically aligned carbon nanofibers produced by plasma-enhanced chemical vapor deposition. *Appl. Phys. Lett.*, vol. 80(3), pp. 476-478.

Mulder, W. H.; Slutyes, J. H.; Pajkossy, T.; Nyikos, I. (1990): Tafel current at fractal electrodes. Connection with admittance spectra. *J. Electroanal. Chem.* vol. 285, pp. 103-115.

Ng, H.T.; Fang, A.; Li, J.; Li, S. F. Y. (2001): Flexible carbon nanotube membrane sensory system: a generic platform. *J. Nanosci. Nanotech.* vol. 1(4), pp. 375-379.

Nguyen, C.V.; Delzeit, L.; Cassell, A. M.; Li, J.; Han, J.; Meyyappan, M. (2002): Preparation of nucleic acid functionalized carbon nanotube arrays. *Nano Letters.* vol. 2(10), pp. 1079-1081.

Ostuni, E.; Chapman, R. G.; Holmlin, R. E.; Takayama, S.; Whitesides, G. M. (2001): A survey of structure-property relationships of surfaces that resist the adsorption of protein. *Langmuir*, vol. 17, pp. 5605-5620.

Penner, R. M.; Heben, M. J.; Longin, T. L.; Lewis, N. S. (1990): Fabrication and use of nanometer-sized electrodes in electrochemistry. *Science*, vol. 250, pp. 1118-1121.

Popovich, N. D.; Thorp, H. H. (2002): New strategies for electrochemical nucleic acid detection. *Interface*, vol. 11 (4), pp. 30-34.

Ren, Z. F.; Huang, Z. P.; Xu, J. W.; Wang, J. H.; Bush, P.; Siegal, M. P.; Provencio, P. N. (1998): Synthesis of large arrays of well-aligned carbon nanotubes on glass. *Science*, vol. 282, pp. 1105-1107.

Rutten, W.; Mouveroux, J.-M.; Buitenweg, J.; Heida, C.; Ruardij, T.; Marani, E.; Lakke, E. (2001): Neuroelectronic Interfacing with cultured multielectrode arrays toward a cultured probe. *Proceedings of The IEEE*, vol. 89(7), pp. 1013-1029.

Shim, M.; Kam, N. W. S.; Chen, R. J.; Li, Y.; Dai, H. (2002): Functionalization of carbon nanotubes for biocompatibility and biomolecular recognition. *Nano Letters*, vol. 2(4), pp. 285-288.

Sosnowski, R. G.; Tu, E.; Butler, W. F.; O'Connell, J. P.; Heller, M. J. (1997): Rapid determination of single base mismatch mutations in DNA hybrids by direct elec-

tric field control. *Proc. Natl. Acad. Sci. U.S.A.*, vol. 94, pp. 1119-1123.

Sotiropoulou, S.; Chaniotakis, N. A. (2003): Carbon nanotube array-based biosensor. *Anal. Bioanal. Chem.* vol. 375, pp. 103-105.

Staros, J. V. (1982): N-hydroxysulfosuccinimide active esters – bis(N-hydroxysulfosuccinimide) esters of 2 dicarboxylic-acids are hydrophilic, membrane-impermeant, protein cross-linkers. *Biochemistry*, vol. 21(17), 3950-3955.

Umek R. M.; Lin, S. W.; Vielmetter, J.; Terbrueggen, R. H.; Irvine, B.; Yu, C. J.; Kayyem, J. F.; Yowanto, H.; Blackburn, G. F.; Farkas, D. H.; Chen Y.-P. (2001): Electronic detection of nucleic acids: a versatile platform for molecular diagnosis. *J. Molec. Diagnosis*, vol. 3 (2), pp. 74-84.

Wightman, R. M. (1981): Microvoltammetric electrodes. *Anal. Chem.*, vol. 53, pp. 1125A-1134A.

Yan, F.; Sadik, O. A. (2001): Enzyme-modulated cleavage of dsDNA for supramolecular design of biosensors. *Anal. Chem.* vol. 73, pp. 5272-5280.

Yu, X.; Chattopadhyay, D.; Galeska, I.; Papadimitrakopoulos, F.; Rusling, J. F. (2003): Peroxidase activity of enzymes bound to the ends of single-wall carbon nanotube forest electrodes. *Electrochem. Comm.*, vol. 5(5), pp. 408-411.